J. Fluid Mech. (1973), *vol.* **60**, *part* 4, *pp.* 703–719
Printed in Great Britain

High-speed water jets from vertically accelerated rotating cones

By P. SAVIC, J. D. ALLAN AND G. P. VAN BLOKLAND
Mechanical Engineering Division, National Research Council, Ottawa

(Received 26 December 1972)

Water jets are produced by vertically accelerating a rotating cone partially filled with water. It is shown that the acceleration of the parabolic meniscus results in a motion similar to that observed in a shaped explosive charge (Monroe jet). Acceleration of the cone is effected by means of an inductive electromagnetic accelerating device (conical pinch) whose theory is developed in terms of the WKB approximation. A second-order inviscid theory for the motion of the fluid in the cone in terms of the Penney–Price linearization procedure is presented and it is shown that good agreement for the jet head velocity can be achieved for low velocities. At higher velocities, experimental results appear to lag behind the theoretical ones, probably owing to the dispersal of the jet head through viscous drag with the surrounding atmosphere. The shape of the jet at early times is well represented by first-order theory.

1. Introduction

High-speed water jets have for some time been used for drilling, cutting and shaping various materials. The advantages of this technique lie in the small width of cuts attainable and the avoidance of the necessity to sharpen the tool. Since most methods of water-jet production comprise a high-pressure pump followed by pipes, nozzles and possibly hydraulic intensifiers, the maximum stagnation pressures attainable in the jets depend on the strength of the walls used to enclose the hydraulic circuit. To overcome this limitation, it has been suggested that some form of hydrodynamic jet intensification involving converging flow be used. One such device is the Monroe jet or shaped charge. In this case an explosive charge containing a conical hole lined with a layer of metal is exploded at the end nearest the apex of the cone. The resulting detonation wave compresses the metal lining, causing it to flow towards the centre-line and along it to form a narrow jet of considerable speed and penetrating power. The theory of this mechanism has been fully explored and tested experimentally (Birkhoff *et al.* 1948; Clark 1949; Pugh, Eichelberger & Rostoker 1952; Singh 1972; Eichelberger & Pugh 1952). As the jet is free-standing it does not require confining walls and hence the problem of wall strength does not arise. Obviously, the repeatibility of such a device is severely limited by the fact that the source of the jet is totally destroyed in the process. For this reason the suggestion has been made that the explosive charge be replaced by a magnetic compression device

and the metal lining by some sort of liquid film. That magnetic pressures of great magnitude can be generated has recently been shown by Bless (1972). It remains to couple the magnetic force in some way to the liquid film. Preliminary experiments in this laboratory, using a layer of mercury, indicated that the liquid becomes unstable under an external magnetic field and no jet is formed. Further experiments using non-conducting fluids contained in a deformable hollow metal cone were equally unsuccessful, as the cone became subject to elastic instability, except in the case of small strain, as will be further discussed below.

As the theory of the Monroe jet uses nothing but ideal, incompressible and inviscid fluid characteristics, it may be argued that a cone lined with a liquid layer and accelerated along its axis is in fact equivalent to a cone that collapses in a manner in which all points on the cone wall approach the centre-line with equal velocity, the only difference being that in the former case an additional shear velocity along the cone wall is imposed, which, since the liquid is assumed inviscid, does not alter the mechanics of the motion. This is the solution adopted in this work, whereby the liquid layer is produced by rotating the cone about its axis. It will be shown in the following that, although the liquid layer produced in in this way is by no means of uniform thickness, the velocity amplification of the resulting jet relative to the cone is considerable and when the parabolic meniscus is tangential to the cone corresponds to the findings of the Monroe jet theory.

The theory of electromagnetic acceleration of a mass due to the discharge of a condenser through a coil has been developed in terms of the Wentzel–Kramers–Brillouin (WKB) approximation and will be reported elsewhere. The most important result of this theory concerns the energy transfer efficiency, i.e. the ratio of the kinetic energy of the mass to the total electrical energy initially stored in the condenser, and its dependence on the applied voltage. Agreement with experimental results is good (figure 1) providing that the effect of the virtual mass of the fluid is taken into account.

The theory of jet motion developed in the following bears some resemblance to the work of Moore & Perko (1965), Bowman (1966), Milgram (1969) and Moody & Reynolds (1971). All of these authors except Milgram were concerned with fluid under the action of accelerations and decelerations. Moore & Perko considered cylindrical vessels with a plane bottom and an initially non-plane free surface. They developed the theory in terms of a semi-analytic expansion procedure, whereby a series of orthogonal functions with time-dependent coefficients was obtained. Bowman linearized the equation of motion about a plane free surface, considering the effect of surface tension on the free-surface pressure distribution. Milgram considered the motion of fluid in a cylindrical tank under the action of a vertical impact and studied the motion of the free surface, initially distorted by interfacial tension at the container wall, in terms of a Taylor-type instability. Moody & Reynolds developed a general computer code for the study of free-surface motion and applied this technique to the sloshing in tanks. There appears, however, to be no analytic solution to the related problem of surface instability in a container with non-cylindrical walls. In what follows, the action

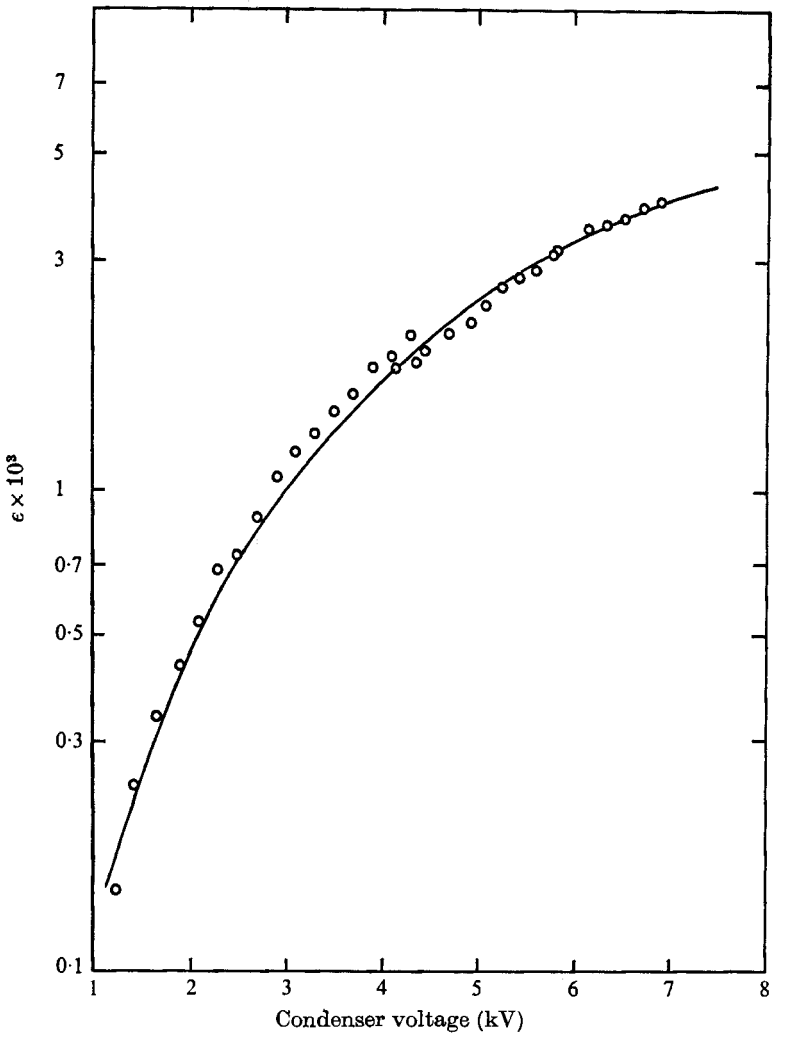

FIGURE 1. Transfer efficiency ϵ *vs.* condenser voltage: comparison with photoelectric speed measurements. ——, theory; ○, experiments.

of acceleration both on an initially distorted free surface and on a conical confining surface will be taken into account. Before attempting a solution of this problem, we shall first study the conditions under which a paraboloidal free surface in a rotating cone can be maintained.

2. Hydrodynamics of jet formation

2.1. *Stability of rotating liquid in a cone*

If a circular cone partially filled with liquid is rotated about its axis, the meniscus of the liquid rises to form a paraboloidal free surface. Contrary to what occurs in a vessel with cylindrical sides, this process cannot be continued to ever-increasing

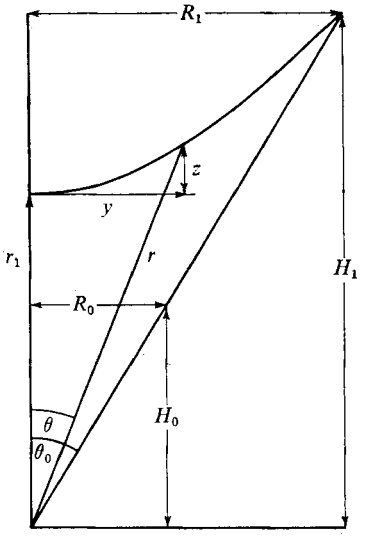

FIGURE 2. Co-ordinate system.

rotational speeds. When the rotational speed reaches a value at which the paraboloid becomes tangential to the side of the cone, the liquid becomes unstable and spills over the edge of the cone. Thus the limit on creation of a liquid layer in this manner is imposed by the existence of a critical rotational speed. We shall calculate this speed from simple geometrical considerations.

Figure 2 shows the cross-section of a half-cone with apex angle θ_0. The height of the liquid at zero rotational speed is H_0 and the radius of its meniscus R_0. When rotated it rises to a height of H_1 and a radius of R_1. Pressure balance at the paraboloidal meniscus demands that the meniscus assumes a shape given by

$$g(H_1 - r_1 - z) = \tfrac{1}{2}\Omega^2(y^2 - R_1^2).$$

Volume integration shows that the volume of the liquid is

$$\tfrac{1}{3}R_1^2\pi H_1 - (R_1^4\pi\Omega^2/4g),$$

where Ω is the angular velocity and g the acceleration of gravity. This volume must equal the volume $\frac{1}{3}R_0^2\pi H_0$ of the unrotated liquid. In addition we have from geometrical considerations

$$\tan\theta_0 = R_1/H_1 = R_0/H_0.$$

From this and the volume balance equation we obtain

$$R_1^4 - 4gR_1^3(\cot\theta_0/3\Omega^2) + 4R_0^3 g(\cot\theta_0/3\Omega^2) = 0.$$

This quartic equation in R_1 has the form

$$X^4 - MX^3 + N = 0.$$

The meniscus is tangential to the cone provided that this equation has two coinciding roots, the condition for which is

$$27M^4 = 256N,$$

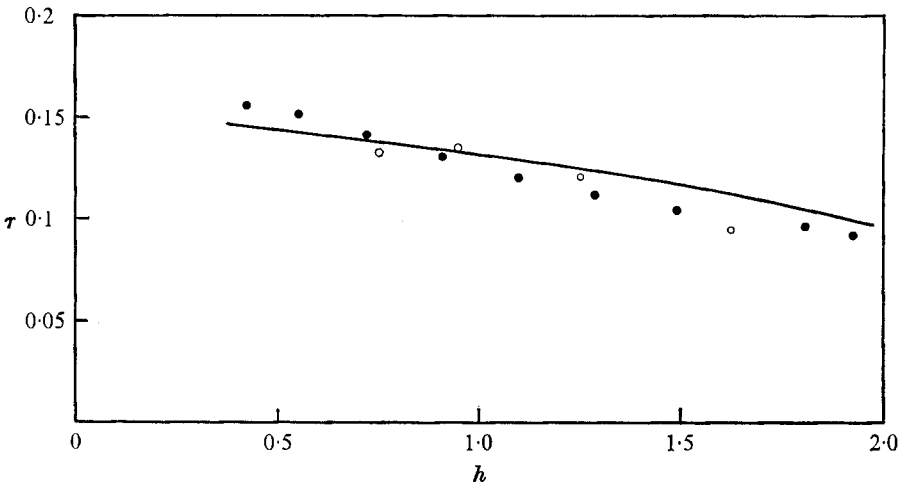

FIGURE 3. Critical rotational period τ of pool of liquid in cone *vs.* initial filling depth. Comparison with experiments. ——, theory. Experiment: ○, water; ●, mercury.

from which the critical rotational speed Ω^* is obtained:

$$\Omega^* = (2^{-\frac{1}{2}} \cos\theta_0)\,(g/H_0)^{\frac{1}{2}}. \tag{1}$$

This relation is shown graphically in figure 3, where the critical speed is plotted against the initial depth $h = H_1 - H_0$. Also shown are experimental points obtained with water and mercury. The agreement may be considered fair in view of the presence of capillary effects and the difficulty in determining the critical point exactly.

2.2. *Jet formation under artificial gravity*

We shall here diverge somewhat from the classical theory of Monroe jet formation, as in our case the liquid layer is not of uniform thickness. An observer moving with the cone will conclude that the meniscus is the proper equilibrium shape resulting from the action of gravitation and the centrifugal force. As the cone accelerates upwards, the observer will experience a sudden increase of apparent gravity and will rightly conclude that the meniscus must assume a different shape. The unsteady motion of this readjustment will cause a jet to develop near the trough of the meniscus which will rapidly move ahead of the edge of the cone. How this motion is influenced by the rotational speed and the filling level of the cone will be analysed in the following.

Since for practical reasons interest is centred mainly on a knowledge of the velocity of the head of the jet, much valuable information can be gained from a linearized analysis. The full problem involving the nonlinear terms in the hydrodynamic equations as well as considerations of a free surface of ever-changing shape requires extensive numerical study and will therefore not be studied here. On the other hand, Penney & Thornhill (1952) have shown that a linearized treatment with initially fixed surfaces may yield valuable information relating to such problems as the collapse of a fluid column under gravity. This approach

will be adopted in the following. The fluid in the cone is considered ideal, inviscid and incompressible and, while the paraboloidal meniscus is formed by rotational effects, all further influence of rotation on the motion is neglected. This latter assumption may be subject to revision in certain cases, as will be shown below.

The essence of the method of Penney & Thornhill lies in the neglect of the velocity convection terms in Euler's equation, together with considering the free surface to be acted upon by the hydrostatic pressure of the fluid column above the lowest point. This simple interface condition arises naturally through expansion of all coefficients of the orthogonal expansion of the velocity potential in terms of a power series in time, retaining only the lowest-order term. To this order in the time expansion the effect of the distortion of the interface from its rest position on the pressure condition need not be taken into account. The fluid adjacent to the other bounding surfaces is subject to the usual conditions of vanishing transverse flow. If all surfaces involved are members of the same orthogonal set of co-ordinate surfaces, the problem is solved at once by the method of eigenfunction expansion. Though, unfortunately, the paraboloidal meniscus and the conical container do not belong to the same co-ordinate system, a two-step approximation procedure has been adopted and was found to give useful information about the motion for the case where the distortion of the free surface is not too great. However, to permit this last step, it is necessary to make the additional assumption that the cone is slender, i.e. that its apex angle is small.

First-order approximation. We adopt the spherical polar co-ordinate system depicted in figure 2. We seek a solution of Laplace's equation for the velocity potential ϕ subject to the boundary conditions

$$\partial\phi/\partial\theta = 0 \quad \text{for} \quad \theta = \theta_0, \tag{2a}$$

$$\partial\phi/\partial t = p/\rho = z\,dV/dt \quad \text{at the free surface.} \tag{2b}$$

The first of these conditions expresses the fact that there is no flow across the surface of the cone. The second, in which p is the pressure, ρ the density and V the vertical velocity of the cone, is derived from the condition of Penney & Thornhill that the pressure on the free surface is equal to the hydrostatic pressure due to the height of the fluid above the parabolic trough.† To first order, the free surface is defined as $r = r_1$. This is in accordance with the assumption that the cone is slender and that the constant radius vector describes an essentially plane surface. The general solution of Laplace's equation can be written thus:

$$\phi = \Sigma A_n (r/R_1)^n P_n(\cos\theta),$$

where the A_n are undetermined constants and the P_n are Legendre functions. Since θ_0 is assumed small, all the running indices (which may be non-integer) will be large. It is therefore permissible to substitute the asymptotic Bessel-function representation for the Legendre functions

$$P_n(\cos\theta) \simeq J_0\{(n+\tfrac{1}{2})\,\theta\}$$

to obtain

$$\phi = \Sigma A_n (r/H_1)^{q_n/\theta_0 - \frac{1}{2}} J_0(q_n\theta/\theta_0), \tag{3}$$

† It is assumed that dV/dt is much larger than g.

where the q_n are the zeros of the Bessel function $J_1(q_n)$. Writing the equation of the parabolic surface in figure 2 as

$$z = \gamma y^2 \quad \text{where} \quad \gamma = \Omega^2/2g,$$

we see that

$$(z/\gamma)^{\frac{1}{2}} = (r_1+z)\tan\theta \simeq (r_1+z)\,\theta,$$

where the tangent has been replaced by its argument in accordance with the slender-cone assumption. Solving for z to second order gives

$$z \simeq \gamma\theta^2 r_1^2,$$

and we obtain for (2*b*)

$$\partial\phi/\partial t = \gamma\theta^2 r_1^2\, dV/dt \quad \text{at the free surface.}$$

Integrating with respect to t yields

$$\phi_{r=R_1} = \gamma V\theta^2 r_1^2. \tag{4}$$

This is the final form of (2*b*). Together with (3) we therefore have

$$\Sigma A_n J_0(q_n\theta/\theta_0) = \gamma V\theta_0^2 r_1^2(\theta/\theta_0)^2.$$

This is Dini's form of a Fourier–Bessel expansion, which can be solved immediately by employing the series representation

$$\Sigma J_0(q_n x)\,\{q_n^{-2}/J_0(q_n)\} = \tfrac{1}{4}x^2,$$

from which it follows that the coefficients of the series are

$$A_n = 4V\gamma\theta_0^2 r_1^2 q_n^{-2}/J_0(q_n).$$

To determine the velocity components on the free surface, we remember that

$$v_r = \partial\phi/\partial r, \quad v_\theta = r^{-1}(\partial\phi/\partial\theta),$$

whence on the free surface

$$v_r = 4V\gamma\theta_0 r_1 F(\theta/\theta_0), \quad v_\theta = 2V\gamma\theta_0 r_1(\theta/\theta_0). \tag{5}$$

The function $F(x)$ is the sum of the series

$$F(x) = \Sigma J_0(q_n x)\,\{q_n^{-1}/J_0(q_n)\}, \tag{6}$$

where the term $-\frac{1}{2}$ has been neglected relative to the much larger values of q_n/θ_0.

Approximate summation of the series $F(x)$. With (5) the first-order problem is formally solved; however, the series (6) is cumbersome and converges slowly. We shall attempt an approximate summation of this series in finite terms. Since the q_n are large numbers, it is admissible to represent $J_0(q_n)$ in terms of its asymptotic value

$$J_0(q_n) \simeq (2/\pi q_n)^{\frac{1}{2}}\cos(q_n - \tfrac{1}{4}\pi), \tag{7}$$

and as $q_n \simeq \pi(n+\frac{1}{4})$ it follows that (6) may be written as

$$F(x) = \tfrac{1}{2}\pi\Sigma J_0(q_n x)\,J_0(q_n).$$

On the other hand we have

$$J_0(\pi n) = \pi^{-1}(2/n)^{\frac{1}{2}}\cos(\pi n - \tfrac{1}{4}\pi) = n^{-\frac{1}{2}}/\pi.$$

Substituting in (6) for $q_n = \pi(n+\frac{1}{4})$ and neglecting $\frac{1}{4}$ under the square root, there results

$$J_0(\pi n) = 2^{-\frac{1}{2}} J_0(q_n). \tag{8}$$

If in (6) the argument $q_n x$ is replaced by $x\pi(n+\frac{1}{4})$ and the addition theorem for Bessel functions is applied to the first two terms, we obtain

$$F(x) = (\pi/2^{\frac{1}{2}})\,\Sigma\{J_0(\pi n)\,J_0(x\pi n)\,J_0(\tfrac{1}{4}x\pi) - 2^{\frac{1}{2}} J_0(q_n)\,J_1(x\pi n)\,J_1(\tfrac{1}{4}x)\}.$$

Consider the first term in this expression, i.e.

$$F_1(x) = \tfrac{1}{2}\pi\,\Sigma J_0(x\pi n)\,J_0(\pi n).$$

Applying the product representation of Bessel functions (Magnus, Oberhettinger & Soni 1966, p. 95)

$$F_1(x) = \tfrac{1}{2}\Sigma \int_0^{\pi} J_0\{\pi n(1+x^2-2x\cos u)^{\frac{1}{2}}\}\,du$$

and the Schloemilch series (Gradshteyn & Ryzhik 1965, p.976, formula(8.521.1))

$$\Sigma J_0(nx) = -\tfrac{1}{2} + (1/x)$$

we can sum the infinite series before evaluating the integral. Further, we use the definite integral (Gradshteyn & Ryzhik 1965, p. 387, formula (3.674.1))

$$\int_0^{\pi} (1-2p\cos u + p^2)^{-\frac{1}{2}}\,du = 2K(p),$$

where $K(p)$ is the elliptic integral of the first kind. Hence, we find that

$$F_1(x) = \tfrac{1}{2}\{-\tfrac{1}{2}\pi + (2/\pi)\,K(x)\}. \tag{9}$$

Since the remaining term is a first-order correction, we are free to replace πn by q_n, again neglecting $\frac{1}{4}\pi$, and we get

$$F_2(x) = \Sigma J_0(q_n)\,J_1(xq_n),$$

or, using the asymptotic value for $J_0(q_n)$ again,

$$F_2(x) = \Sigma\,(2/\pi)\,J_1(xq_n)\{q_n^{-1}/J_0(q_n)\}.$$

This is a summable Dini series:

$$F_2(x) = -\pi^{-1}x.$$

By substituting $F_1(x)$ and $F_2(x)$ in the original expression, we obtain

$$F(x) = 2^{-\frac{1}{2}} J_0(\tfrac{1}{4}x\pi)\{-\pi 2^{-1} + (2/\pi)\,K(x)\} + xJ_1(\tfrac{1}{4}x\pi). \tag{10}$$

As a numerical check we calculate $F(0)$, finding $F(0) = 0{\cdot}40361$, and compare this with the value 0.38485 obtained by direct summation of the series. The error is less than 5%.

Virtual mass ratio. The final efficiency departs from the transfer efficiency calculated above because along with the fluid, a metallic cone has to be accelerated, and by itself does not contribute to the penetrating action of the jet. Moreover, the mass is not to be taken as the actual rest mass of the cone–fluid system but must contain the virtual mass of the fluid created by the flow itself.

We shall now derive a first-order expression for the ratio of the virtual to actual mass of the fluid.

The vertical component of the integrated pressure forces acting on the side of the cone is

$$f_v = 2\pi \int_0^{r_1} rp \sin^2\theta_0 dr = 2\pi\theta^2 \int_0^{r_1} rp\, dr$$

and from the expression for the pressure in terms of the velocity potential and the solution (5)

$$f_v = 8\pi\gamma\theta_0^2 r_1^4 \rho \frac{dV}{dt} \Sigma q_n^{-2} \left(\frac{q_n}{\theta_0} + \tfrac{3}{2}\right)^{-1}.$$

The mass force is

$$f_m = m(dV/dt),$$

whence the virtual mass ratio

$$\frac{f_v + f_m}{f_m} = 1 + 12\Omega^2 r_1 g^{-1} \Sigma q_n^{-2} \left(\frac{q_n}{\theta_0} + \tfrac{3}{2}\right)^{-1}.$$

The infinite series may be summed in terms of the ψ function (logarithmic derivative of the gamma function) to give

$$\frac{f_v + f_m}{f_m} = 1 + \Omega^2 r_1 g^{-1} [1 - 48(9\pi\theta_0)^{-1} \{\psi(\tfrac{5}{4} + 3\theta_0/2\pi) - \psi(\tfrac{5}{4})\}]. \tag{11}$$

Substituting (1) for the angular velocity, one sees that, in the case of a 12° cone, the virtual mass is increased by more than 60 %.

Second-order approximation. The first-order approximation was derived on the assumption that only the pressure force was influenced by the curvature of the free surface and that the resulting flow proceeded as if the interface were plane. We shall now attempt to improve upon this approximation by partially taking account of the fact that the pressure condition (2*b*) is to be applied to the actual shape of the meniscus rather than to its rest condition. We write the equation for the parabolic meniscus in polar co-ordinates as follows:

$$r/H_0 = 1 - \alpha + \beta(\theta^2/\theta_0^2), \tag{12}$$

where α and β are constants depending on the speed of rotation. In the following we shall use a non-dimensional parameter S which fully describes the motion, together with the cone apex angle θ_0:

$$S = \Omega^2\theta_0 H_0/(2g) = Fr/(8Ro^2), \tag{13}$$

where Fr is the Froude number and Ro the Rossby number referred to the characteristic length $\theta_0 H_0$. From the geometrical considerations of § 2.1 it follows that

$$\alpha = \tfrac{1}{2}S\theta_0, \quad \beta = S\theta_0. \tag{14}$$

The procedure to be followed subsequently involves the substitution of (12) in (3), where we have adopted H_0 as reference length in place of H_1, expanding the resulting trinomial to first order according to the binomial theorem and replacing A_n by the sum of the two coefficients representing the coefficients of the Dini series

for x^2 and x^4 multiplied by unknown constants a and b respectively. Since the whole series must equal the pressure on the meniscus and therefore be proportional to x^2, we must adjust the constants a and b in such a way that any terms in x^4 vanish and that the coefficient of x^2 corresponds to that on the right-hand side. Neglecting $-\frac{1}{2}$ again relative to q_n/θ_0, expanding (12) raised to the power q_n/θ_0 to two terms, substituting in (3) and equating this to the pressure (4), we obtain

$$\Sigma(a_n+b_n)\{1-(q_m/\theta_0)(\alpha-\beta x^2)\}J_0(q_n x) = V\gamma\theta_0^2 H_0^2 x^2,$$

where $$a_n = 4aq_n^{-2}/J_0(q_n), \quad b_n = 8bq_n^{-2}(1-8/q_n^2)/J_0(q_n)$$

are respectively the coefficients of the Dini series representing ax^2 and bx^4. Summing the resulting series gives

$$ax-(4a/\theta_0)(\alpha-\beta x^2)F(x)+bx^4 = V\gamma\theta_0^2 H_0^2 x^2, \tag{15}$$

where $F(x)$ is the function given in (10). Note that the term resulting from multiplication of the series for bx^4 with q_n has been omitted, in accordance with order-of-magnitude considerations. $F(x)$ must now be expanded in terms of x^2 and a and b must be chosen such that the x^4 term disappears and the x^2 terms balances the right-hand side of (15). From (10) we find that

$$F(x) = 2^{-\frac{3}{2}}(2-\pi)+\tfrac{1}{2}x^2(1+\tfrac{1}{4}\pi),$$

whence

$$a = \frac{V\gamma\theta_0^2 H_0^2}{1+2\beta(\theta_0)^{-1}2^{-\frac{1}{2}}(2-\pi)-2\alpha\theta_0^{-1}(1+\frac{1}{4}\pi)},$$

$$b = \frac{2\beta V\gamma\theta_0 H_0^2\{1+\frac{1}{4}\times 2^{\frac{1}{2}}+4\times 2^{\frac{1}{2}}(\pi-2)\}}{1+2\beta\theta_0^{-1}2^{-\frac{1}{2}}(2-\pi)-2\alpha\theta_0^{-1}(1+\frac{1}{4}\pi)}.$$

Now, the quantity of greatest interest is the velocity of the head of the jet, i.e. $v_{r0} = v_r(\theta=0) = \partial\theta/\partial r(\theta=0)$. Returning to the series representation of the velocity potential:

$$v_{r0} = \Sigma\left[\frac{4(1-\alpha)^{q_n\theta^{-1}-\frac{3}{2}}a}{\theta_0 q_n J_0(q_n)}+\frac{8b}{\theta_0 q_n J_0(q_n)}\left(1-\frac{8}{q_n^2}\right)\right]. \tag{15a}$$

Note that in the second term the $1-\alpha$ term has been omitted to keep orders of magnitude correct. The first term in this may be written, using the approximate value for q_n and the asymptotic expression for $J_0(q_n)$, as

$$\Sigma\tfrac{1}{2}\pi\exp\{(\pi n\theta^{-1}+\tfrac{1}{4}\pi\theta^{-1}-\tfrac{3}{2})\log(1-\alpha)\}J_0(\pi n)\,2^{\frac{1}{2}}.$$

We expand $\log(1-\alpha) = -\alpha$ and use the Schloemilch series (Magnus *et al.* 1966, p. 131) to the second order:

$$\Sigma J_0(n\pi)\exp(-nu) = -\tfrac{1}{2}+(u^2+\pi^2)^{-\frac{1}{2}}+\tfrac{1}{12}u.$$

The second term in (15*a*) was summed term by term and gave the value 0·77021*b*. Taking all terms together and expanding a and b to first order in α and β we get finally

$$v_{r0}/V = 2^{\frac{3}{2}}(-1+\tfrac{1}{2}\pi)S(1-SU), \tag{16}$$

where

$$U = \frac{\pi^2}{24(-1+\frac{1}{2}\pi)}+\tfrac{1}{8}\pi-\tfrac{3}{4}\theta_0-1-\tfrac{1}{4}\pi-2^{\frac{1}{2}}(\pi-2)+\frac{0{\cdot}77021(1+\frac{1}{4}\pi)}{2^{\frac{1}{2}}(-1+\frac{1}{2}\pi)}.$$

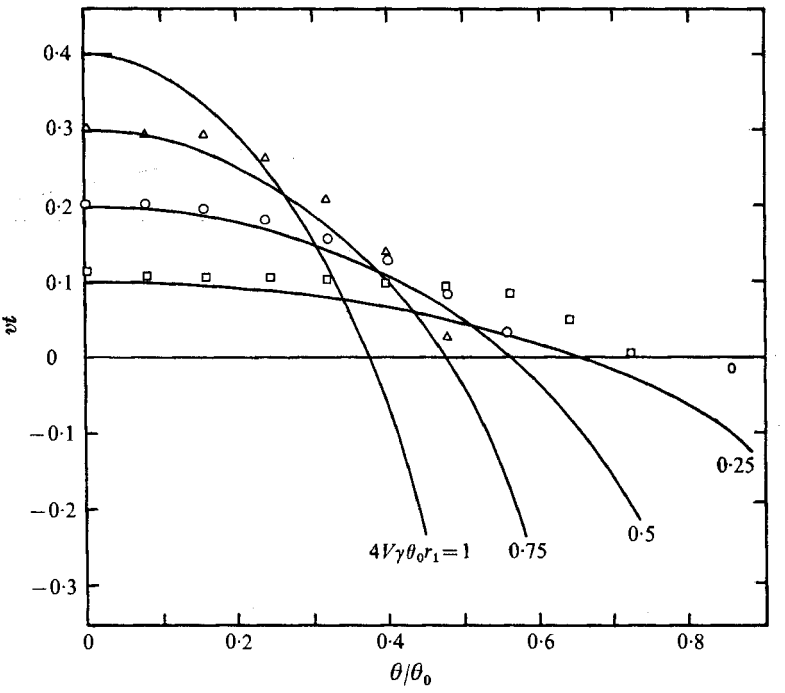

FIGURE 4. Shape of jet for early times: comparison with photographs. ——, theory. Experiment: Δ, $4V\gamma\theta_0 r_1 = 0{\cdot}75$; ○, $4V\sigma\theta_0 r_1 = 0{\cdot}50$; □, $4V\gamma\theta_0 r_1 = 0{\cdot}25$.

This is the second-order expression for the velocity amplification ratio, i.e. the factor by which the velocity of the cone is multiplied to obtain the velocity of the head of the jet. It must be remembered that the whole treatment was carried out in a co-ordinate system travelling with the cone. To convert to a system at rest in the laboratory frame, one must add unity to (16). The largest possible value of this ratio is obtained for the case of critical rotational velocity (1). In this case $S = S_{\max} = 0{\cdot}31498/\theta_0$. In our experiments $\theta_0 = 15\pi$. This yields in the laboratory frame

$$(v_{r0}/V)_{\max} = 6{\cdot}12958.$$

It is interesting to note that to first order in $S_{\max}$, v_{r0}/V becomes inversely proportional to θ_0; this is in agreement with the findings of the classical theory of shaped charges.

Shape of jet profile for small times. From (5) it is possible to obtain the shape of the jet by simply integrating them with respect to time. It must be remembered that in this treatment the convection terms in Euler's equation were neglected; all solutions apply therefore only to small times. Hence, it is not necessary to proceed to the second order in calculating the jet profile, as the first order will yield enough information for the case of low distortion of the free surface.

Figure 4 shows a number of profiles calculated for progressively larger values of time. A distinctive feature of these curves is the rapid negative motion of the fluid near the cone wall. This is due to the logarithmic infinity of $K(x)$ in (10) as x approaches one. In the experiments some breakup of the fluid is observed

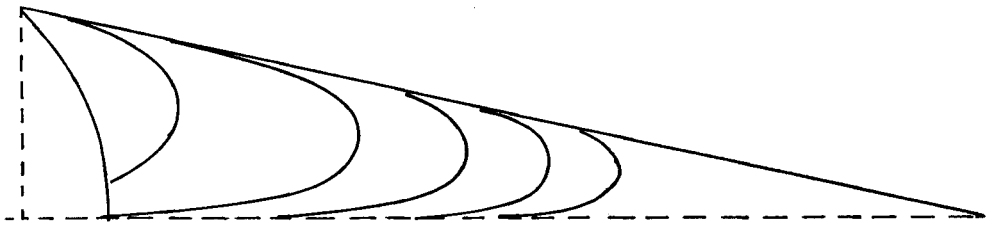

FIGURE 5. Streamline in half-cone for frame at rest in cone.

near this region owing to cavitation caused by the large negative pressures generated. In figure 4 some experimental points taken from photographs of the developing jet are also shown. The agreement appears to be satisfactory in view of the assumptions made and the difficulty in maintaining good experimental conditions. Poorest agreement is found at earliest times, probably owing to the fact that the initial free surface was not plane, as assumed in the first-order theory.

Streamlines. The streamlines of the first-order solution can be obtained from the definition of the stream function ψ:

$$v_r = r^{-2}\theta^{-1}(\partial\psi/\partial\theta), \quad v_\theta = -(r\theta)^{-1}(\partial\psi/\partial r);$$

hence from (5):

$$\psi = \Sigma A_n H_1 \theta(1-\theta_0/2q_n)(r/H_1)^{(q_n/\theta_0)+\frac{1}{2}} J_1(q_n\theta/\theta_0), \tag{17}$$

where the A_n are the coefficients of the Dini series given before. The streamlines are shown plotted in figure 5 for the case of a cone of apex angle 24° ($\theta_0 = 12°$). The large negative velocities near the cone wall are again apparent in this figure, as well as the accumulation of streamlines near the axis of the cone where the jet is formed. It must be noted that the stream function (17) applies to a frame of reference fixed in the moving cone; for a frame stationary in the laboratory, the term

$$\psi_0 = -\tfrac{1}{2}Vr^2\theta^2$$

must be added to (17).

3. Experiments

3.1. *General considerations*

The experimental rig consists essentially of a condenser bank discharging into a conical single-turn coil carrying the rotating cone. The similarity with a plasma pinch (theta pinch) experiment is obvious; however, the design criteria are somewhat different. As in the plasma pinch experiment, the time constant of the discharge must be kept small to ensure that the magnetic field of the coil does not penetrate through the wall of the cone. This is usually achieved by keeping the circuit inductance L_0 as small as possible, a requirement which also guarantees that the inevitable nonlinear change of inductance with cone displacement is kept to a minimum. The theory shows, on the other hand, that the linear change of this quantity should be maximized. To reconcile these two requirements a transformer was designed with a turns ratio of 40:1 and a ferrite core for high-frequency operation. This represented a compromise since a higher turns ratio would involve an intolerable increase in circuit inductance caused by flux leakage.

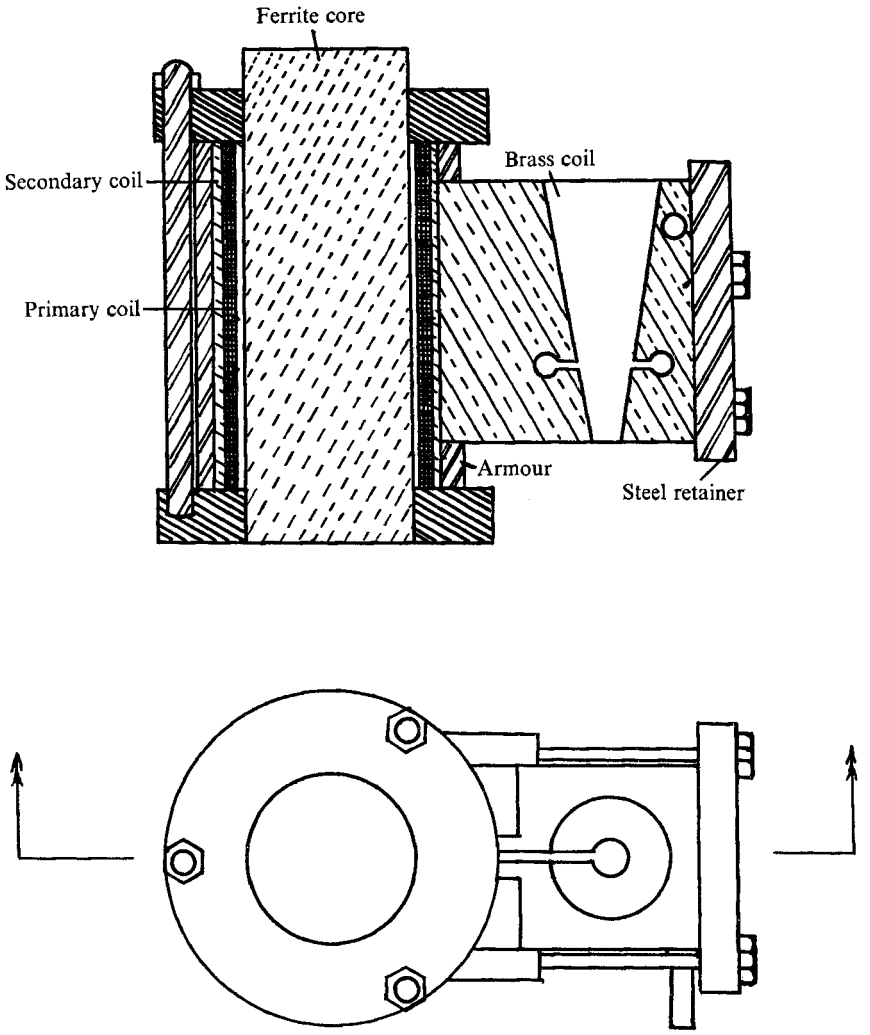

FIGURE 6. Schematic diagram of transformer and coil.

3.2. *Transformer and coil*

A schematic diagram of the transformer is shown in figure 6. The ferrite core is enveloped in a thin layer of mylar sheet insulation which carries the 40-turn primary coil wound with square-section magnet wire. A further layer of insulation separates this from the secondary coil, which is a $\frac{1}{8}$ in. thick split copper tube, which in turn is encased in a $\frac{1}{2}$ in. thick cylinder of steel to prevent the coil from spreading under the action of the magnetic pressure. The conical pinch coil is silver-soldered to the gap in the secondary coil and is held firmly to the transformer by means of a $\frac{1}{2}$ in. retainer plate bolted to two jaws welded to the steel cylinder. The coil itself is a split brass block of square cross-section, carrying a conical hole into which fits the rotating cone. The coil is fitted with an air bearing supplied through a nozzle, while a second nozzle supplies air tangentially to the

cone to provide the torque necessary to make the cone rotate. The transformer is held between two Plexiglas rings and three steel bolts.

The variable inductance L_1 was measured by mounting the cone, made of aluminium, on a traversing rig, the coil being clamped firmly to the base of the ring and the displacement of the cone being measured with a dial gauge. The inductance was measured on a Hewlett–Packard R-X meter (Schering Bridge) using a suitable frequency of the order of a megahertz. The readings had to be modified to take account of the lower working frequencies in the discharge circuit, owing to the greater penetration of the magnetic field.

3.3. *Linear velocity measurements*

The transformer-and-coil assembly was installed in the discharge circuit and the condenser bank charged to a voltage varying between 1200 and 7100 V. The air cushion on which the cone floats is, as a rule, sufficient insulation to prevent the cone from shorting out the coil. For greater safety at high levels of condenser voltage the external surface of the cone was anodized.

The 'muzzle velocity' with which the cone leaves the coil on discharge was measured optically by projecting a collimated beam of light horizontally over the cone, through a 45° glass splitter plate and back again as a parallel beam about 2 in. above the first. The light from this beam, together with a portion of the first beam separated from it by a half-silvered mirror, enters a photodiode, the output of which actuates an electronic interval counter. The discharge current is simultaneously monitored with the aid of a Rogowski coil around one of the conductors, and an oscilloscope. The damped oscillatory signal obtained is analysed to obtain the frequency and, hence, the circuit inductance L_0, while the damping yields the total loss resistance R. As the transfer efficiency was found to be quite small, an approximate expression was used for comparison with experimental values. Results are shown in figure 1. The apparent break in the experimental curve around 4 kV is caused by the fact that, for operation with higher voltages, the pressure supplying the air bearing had to be increased to avoid flash-over between coil and cone, the resulting increase in the air gap giving a small change in the readings.

3.4. *Photographic experiments*

To compare the hydrodynamic calculations with experiment it was necessary to take high-speed photographs of the development of the jet.

A burst of flashes (during $\frac{1}{2}\,\mu$s) illuminates the object while the film of an NRC-Dudgeon drum camera (Dudgeon 1962) is being exposed. This camera has a hollow drum carrying the film on the inside surface and mounted on air bearings and driven by an air turbine. Simultaneously, the rotational speed of the cone is measured by means of a marker painted on the edge of the cone, whose motion is detected by a light- and photo-transistor. The period between successive passages of the marker past the photo pick-up is measured on another interval counter. The rotational speed of the drum camera is monitored on an oscilloscope.

For better photographic contrast the cone was partially filled with milk,

instead of water. Typical results are shown in figure 7 (plate 1), representing shots at different condenser voltages and cone rotational speeds. The voltage seems to have only a minor effect on the shape of the jet, except at high voltage, when the head of the jet seems to develop a plume of spray. This is seen more clearly on figure 8 (plate 2), which shows a single flash picture taken with a still camera. This plume appears to be caused by the drag in the stagnation-point boundary layer of the surrounding air. The resulting loss of fluid and, hence, of apparent forward speed of the jet head causes some difficulty in interpreting the results, as will be seen in the following. In addition, the high-voltage shots also show the development of a thin precursor jet. It is thought that this jet is produced by the elastic contraction of the cone under the magnetic driving field.

It has been assumed in the mathematical analysis that the effect of rotation on the motion of the fluid (as opposed to the development of the meniscus) can be neglected. This is certainly true for early phases of the motion and at high driving voltages. At low voltage and at later times, however, figure 9 (plate 3) definitely indicates rotational effects. These are magnified by the fact that, as can be seen from the streamlines in figure 5, the fluid starting near the wall of the cone is forced towards the centre to form the jet. Owing to the conservation of angular momentum, the angular speed of the fluid composing the jet surface may attain considerable magnitudes. This is shown in figure 9, where the jet edge is seen to be subject to typical centrifugal instability, resulting in the ejection of droplets.

3.5. *Velocity amplification: comparison*

From a technical point of view, the most important quantity is the factor by which the head-of-the-jet velocity is amplified relative to that of the cone, i.e. the velocity amplification. An analytical expression of this quantity is given in (16). Comparison with experimental findings was made simply by measuring the respective slopes of the cone and jet exposures, figure 7. Absolute values of velocity are easily obtained bearing in mind the fact that the flashing rate and, hence, the time between exposures is tightly synchronized with the cycling rate of the counter decade. The scale of the pictures is obtained by exposing a measuring scale in place of the jet. Values of velocity thus obtained are found to agree closely with those measured photoelectrically as described in § 3.3, taking into account the total mass of the cone plus fluid, including the virtual mass. Comparison between the theoretical and experimentally determined velocity amplification *vs.* rotational speed of the cone is made in figure 10. It will be seen that the experimental points agree with the theoretical curve for low values of angular velocity but begin to diverge for higher values, and that the agreement is maintained for higher angular speeds for results obtained with lower driving voltages. This is explained in terms of lateral loss of fluid from the jet head as a result of the dispersal of fluid in the plume. Note that the curves are displaced vertically so that they pass through a point somewhat larger than unity as required by theory. This is due to the fact that even at zero rotational speed the meniscus is somewhat concave, owing to interfacial tension between the fluid and the cone material.

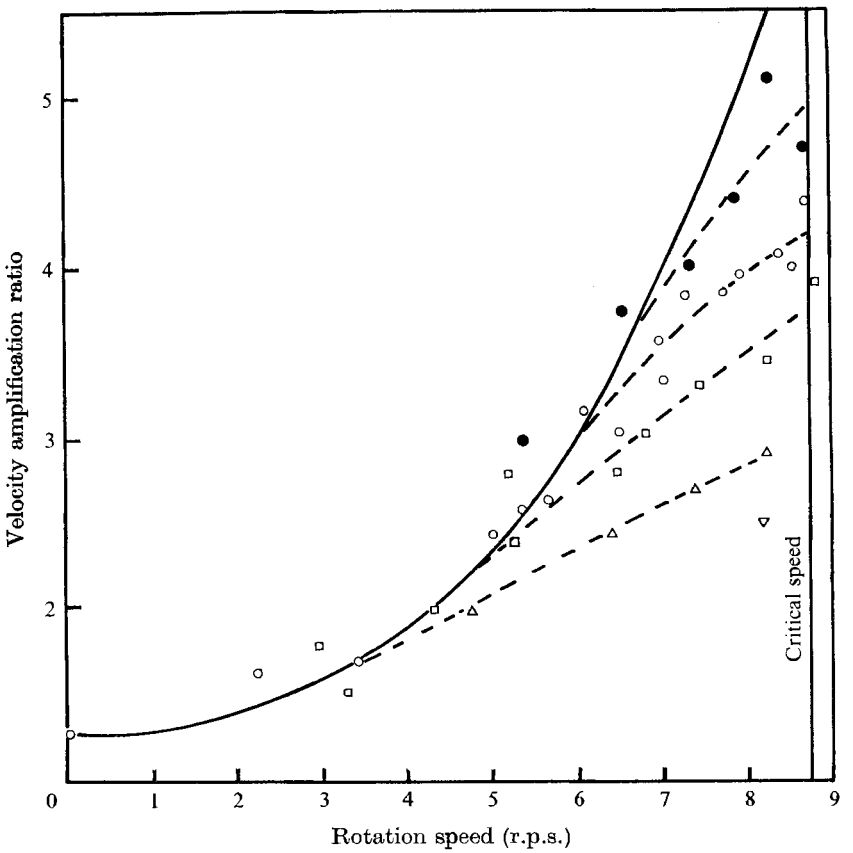

FIGURE 10. Velocity amplification ratio *vs.* rotational speed: comparison of second-order theory with experiments. ——, theory; – – –, experiment. Experimental points; ●, $V_0 = 2$ kV; ○, $V_0 = 3$ kV; □, $V_0 = 4$ kV; △, $V_0 = 5$ kV; ▽, $V_0 = 6$ kV.

4. Conclusions

It is shown that the mechanics of the explosively driven Monroe jet (shaped charge effect) can be simulated by means of a fluid in a rotating and vertically accelerated cone. The theory of the electromagnetic propulsion of the cone by means of a condenser discharge can be developed in terms of the WKB approximation. The hydrodynamic theory, assuming an ideal, inviscid and incompressible fluid, is carried out in a two-step procedure, where the velocity amplification results from a second-order approximation. Good agreement is found with theory for conditions where the velocity of the jet head is comparatively low; at higher velocities the jet tends to be dispersed by frictional interaction with the surrounding air, making the apparent jet velocity somewhat lower than that predicted.

From the point of view of technological application, the coupling between condenser energy and the cone that could be attained in the present experiments was rather poor, resulting in a maximum apparent jet velocity of 230 ft/s (extrapolating for plume loss, this figure may be increased by a factor of 3).

We are greatly indebted to Mr A. J. Bachmeier for suggesting this problem and to Mr M. J. Woodward, Mr B. Mongeau and Mr S. Y. Ho for some preliminary experimental work. Our thanks are also due to Dr I. R. G. Lowe for the design of the air bearing and Dr J. Lau for help with computational work. The technical help of Mr G. Boult, Mr W. C. Michie and Mr J. Margerum is also greatly appreciated.

REFERENCES

ABRAMOWITZ, M. & STEGUN, I. 1965 *Handbook of Mathematical Functions*, pp. 505–507. Washington: Nat. Bur. Stand.

BIRKHOFF, G., MACDOUGALL, D. P., PUGH, E. M. & TAYLOR, G. I., 1948 *J. Appl. Phys.* **19**, 563.

BLESS, S. J. 1972 *J. Appl. Phys.* **43**, 1580.

BOWMAN, T. E. 1966 *Proc. Inst. Environmental Sci. San Diego*, p. 553.

CLARK, J. C. 1949 *J. Appl. Phys.* **20**, 363.

DUDGEON, E. H. 1962 *Proc. 5th Int. Congr. High-Speed Photography*, p. 303.

EICHELBERGER, R. J. & PUGH, E. M. 1952 *J. Appl. Phys.* **23**, 537.

GRADSHTEYN, I. S. & RYZHIK, I. M. 1965 *Tables of Integrals, Series and Products*. Academic.

MAGNUS, W., OBERHETTINGER, F. & SONI, R. P. 1966 *Formulas and Theorems for the Special Functions of Mathematical Physics*. Springer.

MILGRAM, J. H. 1969 *J. Fluid Mech.* **37**, 435.

MOODY, F. J. & REYNOLDS, W. C. 1971 *ASME Preprint*, 71–WA/FE-19.

MOORE, R. E. & PERKO, L. M. 1965 *J. Fluid Mech.* **22**, 305.

PENNEY, W. G. & THORNHILL, C. K. 1952 *Phil. Trans. Roy. Soc.* A **244**, 285.

PUGH, E. M., EICHELBERGER, R. J. & ROSTOKER, N. 1952 *J. Appl. Phys.* **23**, 532.

SINGH, S. 1972 *Ind. J. Pure & Appl. Phys.* **10**, 553.